ORNL/TM-2021/2021

SCALE Modeling of the Fast-Spectrum Heat Pipe Reactor

Erik Walker
Steven Skutnik
William Wieselquist
Alex Shaw
Friederike Bostelmann

May 2022

OAK RIDGE National Laboratory

ORNL IS MANAGED BY UT–BATTELLE, LLC, FOR THE U.S. DEPARTMENT OF ENERGY

ORNL/TM-2021/2021

Nuclear Energy & Fuel Cycle Division

SCALE MODELING OF THE FAST-SPECTRUM HEAT PIPE REACTOR

Erik Walker
Steven Skutnik
William Wieselquist
Alex Shaw
Friederike Bostelmann

Date Published: May 2022

Prepared by
OAK RIDGE NATIONAL LABORATORY
Oak Ridge, TN 37831-6283
managed by
UT-Battelle, LLC
for the
US DEPARTMENT OF ENERGY
under contract DE-AC05-00OR22725

CONTENTS

LIST OF FIGURES

LIST OF TABLES

ACRONYMS

BeO	beryllium oxide
BOL	beginning of life
CE	continuous energy
GWd/MTIHM	gigawatt-days per metric ton of initial heavy metal
HPR	heat pipe–cooled reactor
ICSBEP	International Criticality Safety Benchmark Evaluation Project
INL	Idaho National Laboratory
kW	kilowatt
LANL	Los Alamos National Laboratory
LWR	light-water reactor
MG	multigroup
MW	megawatt
NASA	National Aeronautics and Space Administration
NRC	Nuclear Regulatory Commission
ORNL	Oak Ridge National Laboratory
pcm	percent mille
PIRT	Phenomena Identification and Ranking Table
PWR	pressurized water reactor
SNL	Sandia National Laboratories
SPR	Special Purpose Reactor
SS316	Type 316 stainless steel
UO_2	uranium oxide
VALID	Verified, Archived Library of Inputs and Data

ACKNOWLEDGMENTS

This work was performed under the support of the US Nuclear Regulatory Commission (NRC) under Contract IAA 31310019N0012; the authors wish to gratefully acknowledge the support of the NRC for this work, in particular Hossein Esmaili, Jason Schaperow, Andrew Bielen, Michael Rose, Alice Chung, and program managers Don Algama and Lucas Kyriazidis.

The authors likewise wish to acknowledge the contributions of numerous colleagues who assisted in the development of this work by providing thoughtful feedback and ideas throughout. Specifically, the authors wish to express sincere appreciation to Germina Ilas (ORNL) and Cihangir Celik (ORNL), who provided helpful feedback and discussion throughout the course of this project. In addition, the feedback provided by the MELCOR team, in particular from K.C. Wagner (Sandia National Laboratories) and David L. Luxat (Sandia National Laboratories) was very helpful.

ABSTRACT

As part of the severe accident analysis collaboration with Sandia National Laboratories (SNL) and the Nuclear Regulatory Commission (NRC), SCALE models were developed for a fast-spectrum heat pipe reactor. These models were based on the Idaho National Laboratory (INL) Design A concept, which is an alternative design to the Los Alamos National Laboratory (LANL) Special Purpose Reactor (SPR), also known as the Megapower reactor. The model contains 1,134 heat pipes, surrounded by hexagonal fuel elements, with a potassium working fluid; the fuel is UO_2 with 19.75 wt% ^{235}U enrichment. The model contains axial beryllium oxide (BeO) reflectors above and below the active fuel region along with a radial alumina reflector containing 12 B_4C control drums. The center of the core is left unfueled to make room for two shutdown control rods, one annular and one solid. The active region of the core was discretized into twenty axial and five radial zones to analyze spatial variations in power and burnup.

Infinite lattice unit cell sensitivity studies were used to perform verification between the SCALE and INL models. The eigenvalue results agreed well with the reported results to within roughly 50 percent mille (pcm). Full-core model verification was performed by analyzing system eigenvalues with differing configurations of control drum and shutdown rod positions. These full core results all had eigenvalue differences less than 310 pcm. Control drum and shutdown rod worths were also compared, with differences of 3.2% or less. Using the verified model, the isotopic inventory and decay heat, as well as temperature feedback coefficients, were calculated and provided to SNL as input to the MELCOR severe accident code to analyze potential releases from this class of reactor. The results of the MELCOR analysis are provided in a different report [1].

1. INTRODUCTION

Microreactors have garnered attention recently for their design characteristics that fundamentally differentiate them from traditional large-scale light-water reactor (LWR) designs [2]. With rated thermal energy outputs ranging from 1 to 20 megawatt (MW), microreactors are compact enough to be fully assembled in an offsite factory and then shipped to its operating location via truck, train, or airplane. Because of their small size and ease of mobility, microreactors are perfectly suited for operation in remote outposts, emergency response situations, and forward-operating bases for the military [3], replacing diesel generators. Microreactors are also integral for the future of deep space exploration via nuclear thermal propulsion. Of the various proposed microreactor designs, heat pipe–cooled reactors (HPRs) are particularly well suited for these applications.

Heat pipes are heat transfer devices that have been used for decades in other industries. They transfer heat via a working fluid that requires no pumps or forced circulation. The working fluid is heated within the evaporator portion of the heat pipe, where it is converted to a vapor. As a result of the change in vapor pressure, the vapor flows to the condenser at the opposite end of the heat pipe, where the vapor condenses on the walls of the heat pipe. The newly condensed working fluid then flows back to the evaporator end of the pipe by either capillary action or gravity. This cycle efficiently transfers heat out of the system without the need for pumps or any other moving parts.

This behavior is desirable for nuclear applications because the use of heat pipes prevents large loss of coolant or loss of forced circulations accidents. It is for this reason that there has been much research into the use of heat pipes in nuclear microreactors [4]–[8]. Additionally, commercial vendors are actively developing HPR microreactor designs; Westinghouse is currently developing its eVinci microreactor [9]–[11], whereas Oklo Power is developing its Aurora powerhouse [12], for which it has submitted a combined license application to the US Nuclear Regulatory Commission (NRC) [13].

The increased interest in HPRs and other non-LWR designs makes the ability to accurately model and predict behavior during severe accident scenarios increasingly important as well. To this end, the NRC initiated a project to assess the modeling and simulation capabilities for accident progression, source term, and consequence analysis for non-LWR technologies [14]. This project is a collaboration between the NRC, Oak Ridge National Laboratory (ORNL) and Sandia National Laboratories (SNL); ORNL is using SCALE [15] to provide pertinent data to the MELCOR [16] team at SNL. The SCALE Code System is a modeling and simulation suite for nuclear safety analysis and design that is developed, maintained, tested, and managed by ORNL. MELCOR is a severe accident analysis code developed and managed by SNL that is capable of modeling a broad spectrum of severe accident phenomena in HPRs and other advanced reactor designs.

The SCALE team is tasked with providing the MELCOR team with isotopic inventories, power distributions, decay heat data, and kinetics parameters at the initiation of these severe accidents. This is achieved by using a new inventory interface file generated using the binary isotopic output from SCALE. This generic file type uses standard JSON formatting and can be post-processed into end user–specific inputs such as MELCOR. This work describes the generation of these data and key insights into fast-spectrum HPR microreactors.

2. SCALE MODEL

The Kilopower [17] [18] project was a small, 10 kilowatt (kW) HPR developed by Los Alamos National Laboratory (LANL) and the National Aeronautics and Space Administration (NASA) to power deep-space missions or planetary surface outputs to support human exploration and colonization. The Kilopower design was then scaled up by researchers at LANL to 5 MW thermal and was dubbed the Special Purpose Reactor (SPR), also known as the Megapower reactor [19]. The SPR design consists of heat pipes and uranium oxide (UO_2) fuel enriched to 19.75 wt% ^{235}U. These heat pipe/fuel elements are arranged in a hexagonal array and are placed within channels in a Type 316 stainless steel (SS316) monolithic core structure. However, Idaho National Laboratory (INL) completed a Phenomena Identification and Ranking Table (PIRT) assessment of the LANL concept to identify potential technical and safety issues [20]. This assessment identified issues mainly regarding the SS316 monolith. Therefore, INL proposed two alternatives to the SPR design called Design A and Design B [21]. The HPR design for which a SCALE model was developed in this work is the INL Design A concept.

All neutron transport calculations in this work were performed with SCALE's Monte Carlo code KENO-VI in combination with ENDF/B-VII.0, ENDF/B-VII.1, and ENDF/B-VIII.0 nuclear data libraries in either continuous energy (CE) or multigroup (MG) mode. For depletion calculations, SCALE's TRITON sequence was used, which controls calls to the neutron transport code (i.e., KENO-VI in this case) and the depletion solver ORIGEN. A development version of SCALE 6.3 was used for all calculations.

2.1 INL DESIGN A

2.1.1 HEAT PIPE/FUEL UNIT CELL

The Design A concept incorporates many of the features of the SPR design. It is a 5 MWt fast reactor with a five-year operating lifetime. After five years, the discharge burnup is 2 gigawatt-days per metric ton of initial heavy metal (GWd/MTIHM). The fuel is enriched to 19.75 wt% ^{235}U and is a hexagonal shape surrounding centralized heat pipes oriented vertically. The heat pipe tube and inner and outer fuel claddings are all composed of SS316. The heat pipe working fluid is potassium with 100 g per pipe. The liquid and vapor potassium regions are modeled with differing densities and have constant radii over the entire axial range. There are four He gaps in the model, all of which are 0.0064 cm thick: (1) between the heat pipe tube and the inner fuel cladding, (2) between the inner fuel cladding and the fuel, (3) between the fuel and the outer fuel cladding, and (4) between the outer fuel claddings of neighboring unit cells. The dimensions of this unit cell are given in Table 1 and are depicted in Figure 1.

2.1.2 RADIAL CORE GEOMETRY

There are 1,134 of the aforementioned fuel unit cells in the Design A core. They are arranged into a hexagonal lattice with an inner and outer corrugated SS316 support structure. The center of the core is left unfueled, making room for two emergency B_4C shutdown rods. One shutdown rod is solid, whereas the other is annular, allowing for both rods to be inserted at the same time from the bottom of the core (see bottom part of Figure 3). Outside the core's fueled region, there is a gap and then a radial alumina (Al_2O_3) reflector region. Embedded within the radial reflector region are 12 rotatable B_4C control drums enriched to 90 wt% ^{10}B for reactivity control. Outside the alumina reflector, there is a 1 cm He gap followed by a 5.08 cm thick SS316 core barrel. Surrounding the core barrel is a 15.24 cm thick B_4C radiation shield. The radial dimensions used in this model are given in Table 2. The radial layout of this model is shown in Figure 2.

Table 1. Heat pipe/fuel unit cell dimensions (cm) [21]

Potassium vapor radius	0.7100
Potassium liquid radius	0.7875
SS316 heat pipe tube radius	0.8875
Helium heat pipe gap radius	0.8939
SS316 inner fuel clad radius	0.9339
Helium inner fuel clad gap radius	0.9403
UO_2 fuel radius (center to flat)	1.2802
Helium outer fuel gap radius (center to flat)	1.2866
SS316 outer fuel clad radius (center to flat)	1.3866
Helium unit cell gap radius (center to flat)	1.3930
Unit cell pitch (flat to flat)	2.7860

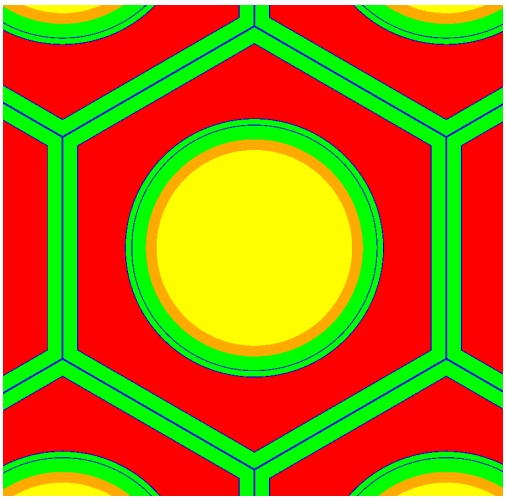

Figure 1. SCALE model of INL Design A unit cell configuration. The fuel is displayed in red, the SS316 clad and heat pipe tube in green, the four gaps in blue, the liquid potassium in orange, and the vapor potassium in yellow.

Table 2. INL Design A core radial dimensions (cm) [21]

B_4C solid control rod radius	5.6
B_4C annular control rod inner radius	6.85
B_4C annular control rod outer radius	8.85
Helium inner radius for control rods	9.05
SS316 outer core radius (center to flat)	49.70
Helium outer core gap radius	50.10
Alumina radial reflector radius	77.85
Helium outer reflector gap radius	78.85
SS316 core barrel radius	83.93
B_4C outer radiation shield radius	99.17

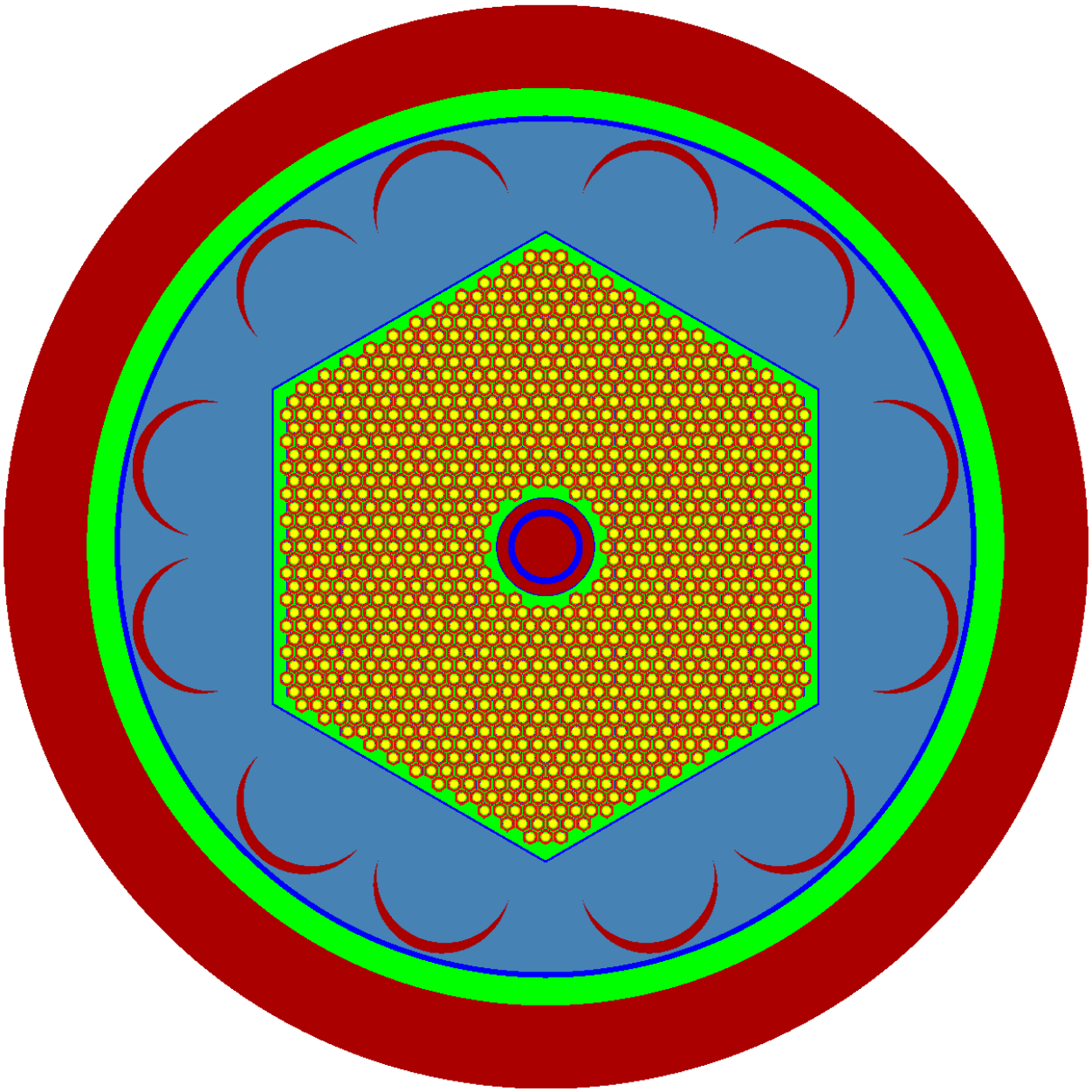

Figure 2. SCALE model of INL Design A core radial layout with control rods inserted. Dark blue represents the voided region and gaps, maroon are the B_4C control drums, control rods, and radial neutron shield, light blue is the alumina reflector, and green is the SS316 core barrel and corrugated support structure. The fuel is still red, the liquid potassium is orange, and the vapor potassium is yellow.

2.1.3 CONTROL DRUM MODELING

The B_4C arcs of the control drums are modeled by placing two 12.5 cm radius cylinders offset from one another by 2 cm. This leads to a maximum arc thickness of 2 cm. The control drums are in their most removed configuration when the thickest part of the B_4C is farthest away from the center of the core rather than the closest flat side of the outer clad support structure. Specifically, this deactivated configuration corresponds to the largest radial distance from the thickest portion of the arc relative to the center of the core. The center of the 12.5 cm control drum cylinders are placed in the reflector relative to the center of the model using the coordinates provided in Table 3.

Table 3. Control drum placement relative to origin at the center of the model

Control drum	**Coordinates**		**Fully withdrawn angle**
	x (cm)	y (cm)	degrees
1	63.10	14.35	12.812
2	44.1074	47.3962	47.058
3	18.9926	61.8962	72.942
4	−18.9926	61.8962	107.058
5	−44.1074	47.3962	132.942
6	−63.10	14.35	167.188
7	−63.10	−14.35	192.812
8	−44.1074	−47.3962	227.058
9	−18.9926	−61.8962	252.942
10	18.9926	−61.8962	287.058
11	44.1074	−47.3962	312.942
12	63.10	−14.35	347.188

2.1.4 AXIAL CORE GEOMETRY

The total axial height of the INL Design A core is 200 cm. The SS316 support structure, barrel, and cladding, as well as the neutron shield, central control rod region, alumina reflector, and control drums, span the full length of the core. Within the SS316 cladding of a heat pipe/fuel element, there is a fission gas plenum located at the very bottom of the core. Above this region is a BeO lower reflector, above which the active fuel region is located. Above the fuel region of the core is another BeO axial reflector. The heat pipes extend from the bottom of the fueled region of the core up through the top, out to a secondary heat exchanger. Because this region is neutronically insignificant, the heat pipes are modeled only to the top of the core in this work. The axial thicknesses of each of these regions is given in Table 4. A visual rendering of the axial profile of the core from flat-to-flat through the center of the core is shown in Figure 3.

Table 4. INL Design A core axial thicknesses (cm) [21]

Helium lower fission gas plenum	20.0
BeO lower axial reflector	15.0
UO_2 fueled region	150.0
BeO upper axial reflector	15.0
Heat pipe region	165.0

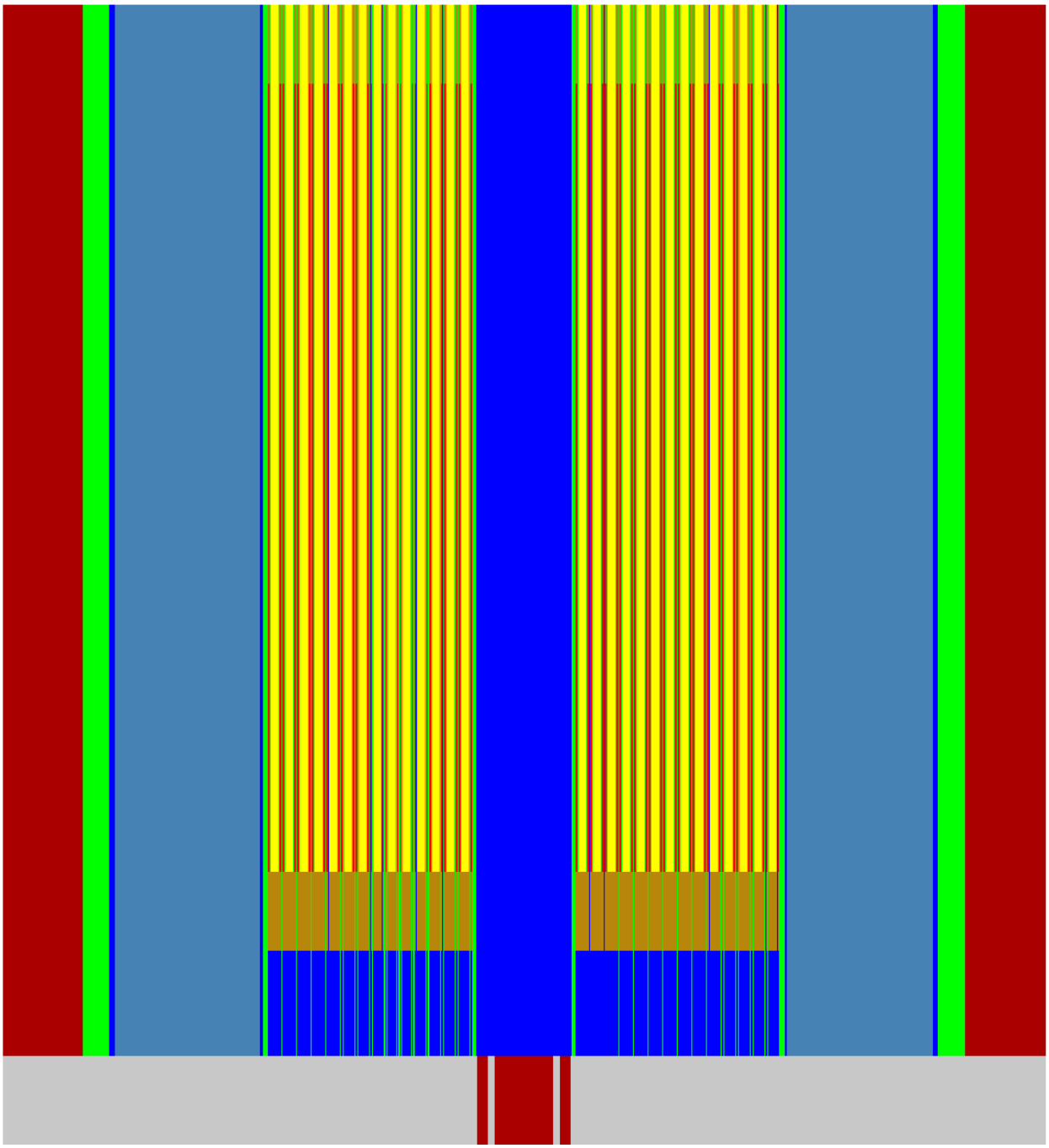

Figure 3. SCALE model of INL Design A core axial layout with control rods withdrawn (full length of control rods not shown). The brown regions represent the upper and lower BeO reflectors, and the gray region below the core is void. All other colors correspond to the same materials as they did in Figure 2: the fuel is red, the SS316 clad and heat pipe tubes are green, the liquid potassium is orange, the vapor potassium is yellow, the voided regions and gaps are dark blue, the B_4C control drums, control rods, and radial neutron shield are maroon, the radial alumina reflector is light blue, and the SS316 core barrel and corrugated support structure are also green.

2.2 DIFFERENCES BETWEEN THE SCALE AND THE REFERENCE MODEL

Although the geometry of this SCALE model is as close to the INL reference design as could be inferred, as described by Sterbentz et al. [21], there are a few key material and modeling differences. The reference document gives the isotopic number densities for each material used in the model. Models were generated using these isotopics, as well as using the built-in SCALE Standard Composition Library. In addition to explicit specifications of nuclide-wise number densities (at/b-cm), SCALE permits convenient specifications of material compositions such as those for SS316. To assess the differences between these material definitions, comparison calculations with explicit nuclide densities and SCALE material definitions were performed. Another key difference is the choice of CE nuclear data library. The reference results were all generated with ENDF/B-VII.0 data. The results presented here were generated using the newer ENDF/B-VII.1 library, unless otherwise noted; some comparisons were done with ENDF/B-VII.0 and ENDF/B-VIII.0 libraries.

2.2.1 MODEL DISCRETIZATION

To accurately capture power and temperature effects within the core, a discretization of the fueled region of the core was performed. The final radial discretization contained five regions, as shown in Figure 4. They were selected to be as close to equal thicknesses as possible; the inner four regions are all three unit cells thick while the outer region is two unit cells thick. From the inner to the outer fuel region, they contain 102, 186, 258, 330, and 258 fuel unit cells, respectively. The axial discretization is given in Table 5. The axial discretization is symmetric about the midplane—except for the bottom plane, which was subdivided an additional time, unlike the top. This was done to better capture the lower reflector peak described in Section 4.1.

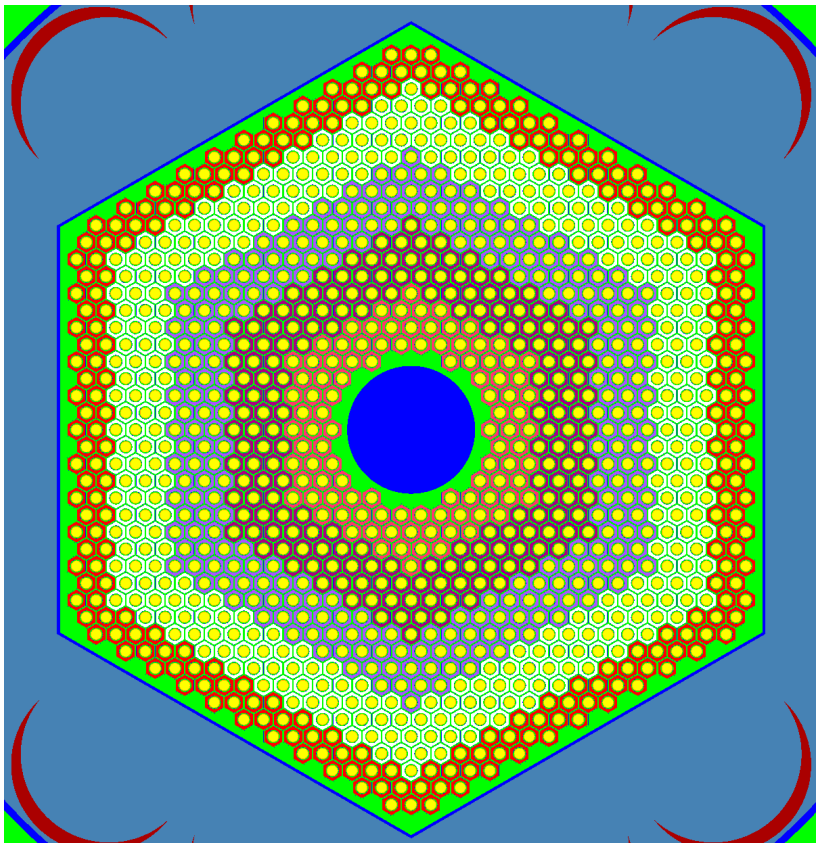

Figure 4. SCALE visualization of radial discretization of the fuel region into five zones.

Table 5. Axial fuel discretization

Plane Number	Axial Thickness (cm)
1 (top)	3.0
2	3.0
3	3.0
4	3.0
5	3.0
6	15.0
7	15.0
8	15.0
9	10.0
10	10.0
11	10.0
12	15.0
13	15.0
14	15.0
15	3.0
16	3.0
17	3.0
18	3.0
19	1.5
20 (bottom)	1.5

2.2.2 MATERIAL TEMPERATURES

An iterative approach was taken to determine the fuel temperatures in the model. With a range of potential operating temperatures listed in the reference document [21], a uniform temperature distribution was initially used. All fuel material temperatures were set at a constant 1,000 K, regardless of position in the core, whereas all other materials were modeled at 950 K. The fuel temperature of 1,000 K was chosen because it is near the upper limit operating temperature provided in Sterbentz et al. [21]. This uniform temperature case was used to generate a power profile that was then given to the MELCOR team at SNL. Based on this power profile, the MELCOR team was able to provide the resulting fuel temperature distribution, which was then used to for a second iteration of the SCALE model [1]. Though the SCALE and MELCOR model discretizations are not the same, a volume-weighted average was used to transfer the MELCOR temperature distribution to SCALE. The fuel temperatures used for each of the 100 fuel regions (5 radial by 20 axial) are given in Table 6. The volume-weighted average fuel temperature for the entire core is 1,061.17 K.

2.2.3 REFLECTOR AND PLENUM REGIONS

The exact geometry of the reflector and plenum regions is not explicitly given in the reference document [21]. Therefore, these regions were created using assumptions that may differ from the INL models. The radial layout of these regions is shown in Figure 5, where the colors represent the same materials as those discussed above. Since the heat pipes extend out the top of the core to the heat exchanger, the upper reflector in Figure 5a simply surrounds the heat pipe while all gap and cladding remain the same as the active fuel region. However, the lower reflector region in Figure 5b does not contain the heat pipe, so the heat pipe region is replaced with more reflector. The lower plenum region in Figure 5c is similar to the lower reflector; all reflector material is replaced with He gap material.

Table 6. Fuel temperature distribution (K) for each region based on temperatures predicted by MELCOR [1]

		Radial Region Number				
		1 (inner)	2	3	4	5 (outer)
Axial Plane Number	1 (top)	1096.48	1081.35	1062.44	1040.85	1023.73
	2	1096.93	1081.74	1062.78	1041.12	1023.94
	3	1097.53	1082.27	1063.23	1041.48	1024.24
	4	1098.26	1082.92	1063.78	1041.93	1024.61
	5	1099.10	1083.66	1064.42	1042.45	1025.03
	6	1102.08	1086.31	1066.70	1044.29	1026.56
	7	1107.55	1091.19	1070.89	1047.69	1029.38
	8	1112.17	1095.32	1074.44	1050.57	1031.79
	9	1114.51	1097.42	1076.25	1052.04	1033.02
	10	1115.14	1097.98	1076.73	1052.43	1033.34
	11	1114.59	1097.50	1076.32	1052.10	1033.06
	12	1112.41	1095.55	1074.64	1050.74	1031.93
	13	1108.18	1091.77	1071.39	1048.09	1029.72
	14	1103.46	1087.54	1067.74	1045.12	1027.25
	15	1101.16	1085.48	1065.97	1043.66	1026.04
	16	1100.59	1084.97	1065.52	1043.30	1025.74
	17	1100.16	1084.58	1065.19	1043.02	1025.52
	18	1099.88	1084.33	1064.97	1042.83	1025.37
	19	1099.78	1084.25	1064.89	1042.76	1025.32
	20 (bottom)	1099.78	1084.25	1064.89	1042.75	1025.32

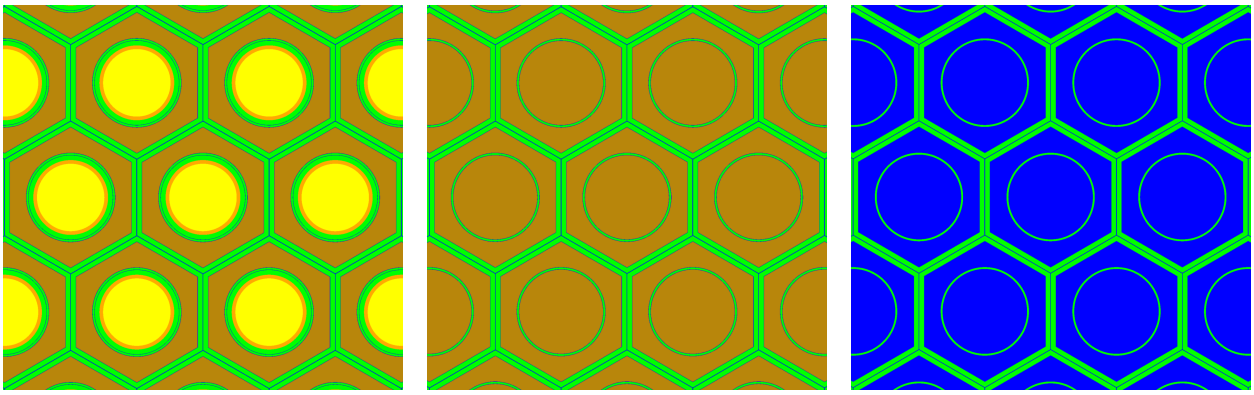

(a) Upper reflector **(b) Lower reflector** **(c) Lower plenum**

Figure 5. SCALE visualization of upper and lower region definitions.

The densities of the radial Al_2O_3 and axial BeO reflectors also differed from the reference document. Since density to number density conversions can be different based on material library, using the provided 3.9 g/cm^3 Al_2O_3 and 3.01 g/cm^3 BeO densities with the SCALE Standard Composition Library resulted in different isotopic compositions from the number densities provided in the report. Therefore, the densities were reduced to 3.7 g/cm^3 and 2.86 g/cm^3 for the Al_2O_3 and BeO reflectors, respectively. These new densities yielded material number densities that aligned more closely with those in the report. The material densities were only changed for the reflectors; all other materials were kept with consistent with those in the reference.

3. MODEL VERIFICATION AND VALIDATION

To ensure consistency between the SCALE model of the INL Design A microreactor and the MCNP® [22] model used in the reference document [21], a series of verification studies were performed. Similarly, some validation studies were performed to compare this SCALE model to previously conducted physical experiments.

3.1 VERIFICATION

3.1.1 UNIT CELL PITCH AND CLAD THICKNESS STUDY

A unit cell comparison was performed, analyzing the sensitivity of the eigenvalue on pitch and clad thickness of the INL Design A core. The unit cells were modeled with reflective boundary conditions, simulating an infinite lattice calculation. The unit cell was assumed to be one radially reflected heat pipe/fuel lattice element from the full core, spanning the full 150 cm height of the active core region with vacuum upper and lower boundary conditions. Three cases were examined in which the unit cell pitch and outer SS316 clad were adjusted. These three cases were modeled twice: (1) with matching detailed isotopics and ENDF/B-VII.0 CE library from the reference document, and (2) using the SCALE Standard Composition Library (i.e., the simplified material input) and the ENDF/B-VII.1 CE nuclear data library. The temperatures of all materials were set to a constant 1,200 K. The calculations were converged to less than 10 pcm eigenvalue uncertainties.

The obtained k_{inf} eigenvalues are provided in Table 7 and are compared to MCNP results reported in [21]. When comparing the SCALE and MCNP results for the models with identical isotopics and CE library, the results are in good agreement; the SCALE model is roughly 50 pcm higher for all three cases. When using different isotopics and the newer ENDF/B-VII.1 CE library, the SCALE models are, on average, 99 pcm higher than the reference. These results show that the SCALE unit cell model is comparable to the reference MCNP model. Therefore, a full-core model was created for verification purposes.

Table 7. Unit cell pitch and clad sensitivity study results. Differences in parenthesis are in pcm

Case	Outer SS316 clad (cm)	Pitch (cm)	k_{inf} (MCNP [21]) ENDF/B-VII.0	k_{inf} (SCALE) ENDF/B-VII.0, Isotopics	Diff. (pcm)	k_{inf} (SCALE) ENDF/B-VII.1, Std. Comp.	Diff. (pcm)
1	0.1	2.786	1.25953	1.25994 ± 0.000096	41	1.26046 ± 0.000069	93
2	0.05	2.786	1.27496	1.27545 ± 0.000079	49	1.27580 ± 0.000087	84
3	0.05	2.686	1.28830	1.28886 ± 0.000093	56	1.28949 ± 0.000088	119

3.1.2 FULL-CORE EIGENVALUE AND REACTIVITY VERIFICATION

A full-core 3D model was created using the details outlined in Section 2.1. This model was used to verify the eigenvalues of different configurations of the control drums and emergency shutdown rods and their worths. When both shutdown rods are inserted and all 12 control drums are rotated closest to the center of the core, this is referred to as *All Poisons In*; when both rods are removed and all control drums are rotated fully away from the center of the core, this is considered *All Poisons Out*. The core excess reactivity at beginning of life (BOL) was also calculated. Similar to what was done for the unit cell verification study performed in the previous section, each configuration was run twice, once with identical isotopics and CE library and once with an updated library and using the SCALE Standard Composition Library. In the SCALE cases, all material temperatures were set to 1,200 K, except the radial alumina reflector, which was set to 600 K. A

summary of these comparisons is given in Table 8. All cases in this study were converged to less than 10 pcm, and these errors were propagated for all reactivity and worth calculations.

As seen in Table 8, both SCALE models agree with the reference MCNP models with eigenvalue differences of, on average, 236 pcm. Similarly, the delayed neutron fraction, β_{eff}, agrees very well with the reported value within 26 pcm. The control drum and shutdown rod worth comparisons show differences of 3.7% or less, whereas the excess reactivity comparison shows much larger percent differences. These differences are likely due to the modeling assumptions described in Section 2.2.

Table 8. Full-core eigenvalue and reactivity comparison results

Control Condition/Parameter	Ref. MCNP	SCALE ENDF/B-VII.0, Isotopics	Difference (pcm or %)	SCALE ENDF/B-VII.1, Std. Comp.	Difference (pcm or %)
All Poisons Out	1.02825	1.03131 ± 0.000089	306	1.03144 ± 0.000087	319
All Poisons In	0.84594	0.84742 ± 0.000088	148	0.84692 ± 0.000082	98
Control Drums In	0.95042	0.95238 ± 0.000086	196	0.95230 ± 0.000089	188
Annular Shutdown Rod In	0.94555	0.94840 ± 0.000090	285	0.94834 ± 0.000092	279
Solid Shutdown Rod In	0.95933	0.96200 ± 0.000093	267	0.96208 ± 0.000093	275
β_{eff}	0.007	0.00713 ± 0.000120	13	0.00726 ± 0.000120	26
BOL Excess Reactivity ($)	3.92	4.259 ± 0.069846	8.3%	4.200 ± 0.068015	6.9%
Total Drum Worth ($)	11.38	11.273 ± 0.184879	−0.9%	11.103 ± 0.179782	−2.5%
Individual Drum Worth ($)	0.97	1.002 ± 0.016440	3.2%	0.980 ± 0.015874	1.0%
Annular Shutdown Rod Worth ($)	12.15	11.892 ± 0.195030	−2.1%	11.708 ± 0.189575	−3.7%
Solid Shutdown Rod Worth ($)	9.98	9.801 ± 0.160738	−1.8%	9.632 ± 0.155966	−3.5%

3.1.3 FULL-CORE REACTIVITY FEEDBACK COEFFICIENT VERIFICATION

The reference document [21] cites four primary negative reactivity feedback effects with INL Design A: (1) doppler coefficient of the UO_2 fuel, (2) axial thermal expansion of the UO_2 fuel, (3) radial thermal expansion of the alumina reflector, and (4) radial thermal expansion of the outer SS316 fuel cladding. The thermally expanded dimensions were determined using

$$L_f = L_i + L_i \cdot \alpha_{avg} \cdot \Delta T, \tag{1}$$

where L_f and L_i are the final and initial dimensions, respectively, α_{avg} is the mean thermal expansion coefficient, and ΔT is the temperature difference across which the expansion occurs.

Doppler Broadening

As the fuel temperature increases, neutron resonances broaden, increasing resonance absorption. This is the primary negative reactivity feedback effect in the INL Design A core. The Doppler coefficient was calculated by running a series of calculations with differing uniform fuel temperatures. The temperatures included were 300 K, 600 K, 900 K, 1,200 K, 1,500 K, 1,800 K, 2,100 K, and 2,400 K. Points at 1,000 K and 1,061.17 K were also included because they were used in the two model iterations, as described in Section 2.2.2. All cases were converged to eigenvalue uncertainties of less than 5 pcm. The reactivity response as a function of fuel temperature is expected to be logarithmic [23], so a log fit was applied. The data points, log fit, and error bars are shown in Figure 6. Although the uncertainties are included in Figure 6, they may be difficult to see because they are roughly the same size as the data points themselves. The Doppler coefficient was calculated by taking the derivative of the log fit at 1,061.17 K, the volume-averaged fuel temperature.

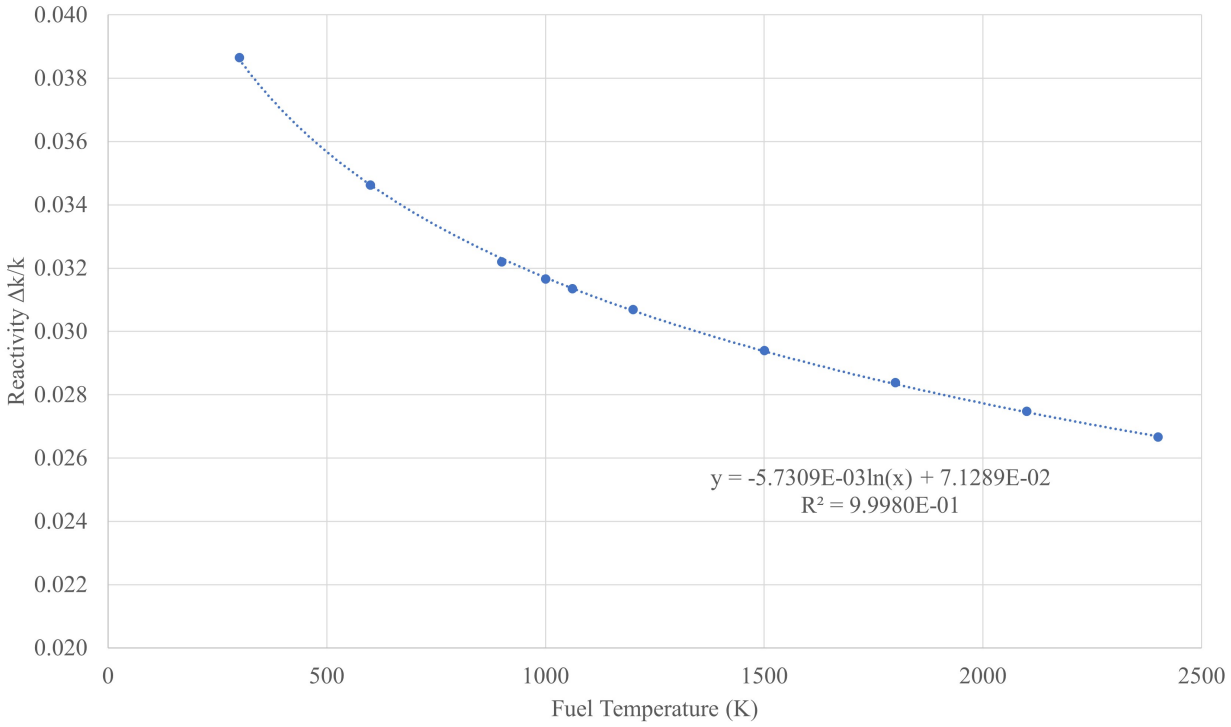

Figure 6. Temperature dependence of reactivity shown with log fit and error bars.

Axial Fuel Thermal Expansion

As the fuel heats up and expands, the larger volume reduces the overall density of the UO_2 fuel. For this study, fuel expansion is only considered in the axial direction; the radial dimensions are kept constant. Since the fission gas plenum in INL Design A is located at the bottom of the core, it is assumed that the fuel expansion will occur downward. However, the lower BeO reflector is located directly below the fuel and above the plenum. Therefore, when the fuel expands axially downward, it pushes the lower BeO reflector downward as well by the same amount. All other material dimensions are kept constant, and any new gaps created are filled with the He fill gas. A depiction of this axial expansion is given in Figure 7. Using Table 1.5 from Appendix C of the reference document [21] and linear interpolation, a thermal expansion coefficient of 1.00933E-05 m/m·K was used corresponding to an expansion from 273 K to 1,061.17 K, the volume-averaged fuel temperature. This yielded a fuel length increase of 1.1933 cm, reducing the overall UO_2 fuel density from 10.52 g/cm^3 to 10.437 g/cm^3. The fuel temperatures were held constant at the values given in Table 6, and only the fuel densities were allowed to change.

Radial Alumina Thermal Expansion

As the alumina reflector thermally expands radially, it simultaneously moves farther away from the core and reduces its density as it expands. This leads to an increase in radial leakage out of the core, thus reducing the overall reactivity. Also, while the alumina is expanding outward, the twelve radial control drums contained within the radial reflector are also shifting outward, further decreasing reactivity. For this study, only radial expansion is considered; all axial dimensions are kept constant. A thermal expansion coefficient of 8.50E-06 m/m·K was used for 99.9% pure commercial-grade alumina [24]. Using Eq. (1), an expansion was performed from 293 K to 950 K, the assumed alumina temperature. The center-to-flat radius of the inner alumina surface expanded from 50.1 cm to 50.3798 cm, whereas the outer radius expanded from 77.85 cm to 78.2848 cm. This resulted in a decrease in the alumina density from 3.7 g/cm^3 to 3.6590 g/cm^3. The

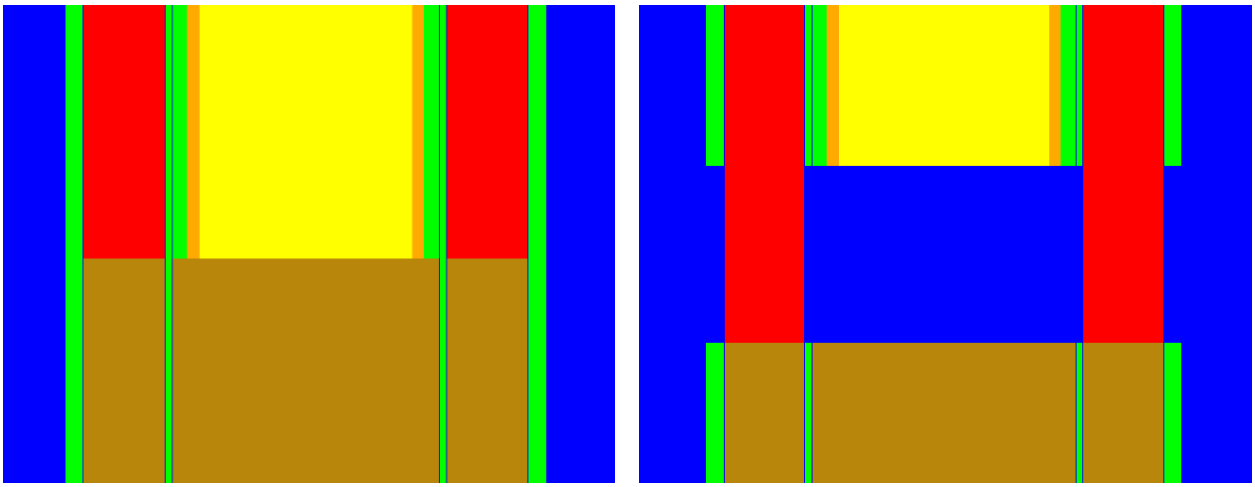

(a) Before expansion **(b) After expansion**

Figure 7. SCALE visualization of axial view of fuel expanding downward, pushing the BeO reflector down as well.

new thermally expanded control drum positions are given in Table 9. The fully withdrawn angles remain the same as those in Table 3 since the control drums move radially away from the center of the core.

Table 9. Thermally expanded control drum placement relative to origin at the center of the model

Control Drum	**Coordinates**		**Fully withdrawn angle**
	x (cm)	y (cm)	degrees
1	63.4524	14.4301	12.812
2	44.3537	47.6609	47.058
3	19.0987	62.2419	72.942
4	−19.0987	62.2419	107.058
5	−44.3537	47.6609	132.942
6	−63.4524	14.4301	167.188
7	−63.4524	−14.4301	192.812
8	−44.3537	−47.6609	227.058
9	−19.0987	−62.2419	252.942
10	19.0987	−62.2419	287.058
11	44.3537	−47.6609	312.942
12	63.4524	−14.4301	347.188

Radial SS316 Clad Thermal Expansion

When the temperature of the outer fuel cladding increases, the SS316 thermally expands, increasing the outer dimension of the fuel unit cell. Eventually, the clad expands to a point at which the gap between neighboring unit cells closes. Continued expansion causes the unit cells to push on each other, increasing the pitch between them and increasing the outer dimension of the corrugated SS316 support structure. The pitch increases so much that the gap between the core and the surrounding alumina reflector also closes. Therefore, unlike the reference document, the SCALE model does not simulate the thermal expansion of the fuel cladding alone, but instead models all radial thermal expansion effects simultaneously since they are so closely coupled. For this study, only radial expansion is considered; all axial dimensions are kept constant.

Using Table 1.1 from Appendix C of the reference document [21], a thermal expansion coefficient of 1.91E-05 m/m·K was used to expand from 293 K to 950 K. Using Eq. (1), the center-to-flat radius of the inner dimension of the clad increased from 1.2866 cm to 1.3028 cm, whereas the outer dimension increased from 1.3866 cm to 1.4040 cm. Therefore, the total fuel unit cell pitch increased from 2.786 cm to 2.808 cm. The outer corrugated SS316 support structure was also thermally expanded from 49.7 cm to 50.3237 cm, center-to-flat. All SS316 densities were reduced from 7.928 g/cm^3 to 7.733 g/cm^3 while the outer fuel element gaps were completely removed from the model, as shown in Figure 8. The radial alumina thermal expansion was then incorporated using the same values described in the previous section.

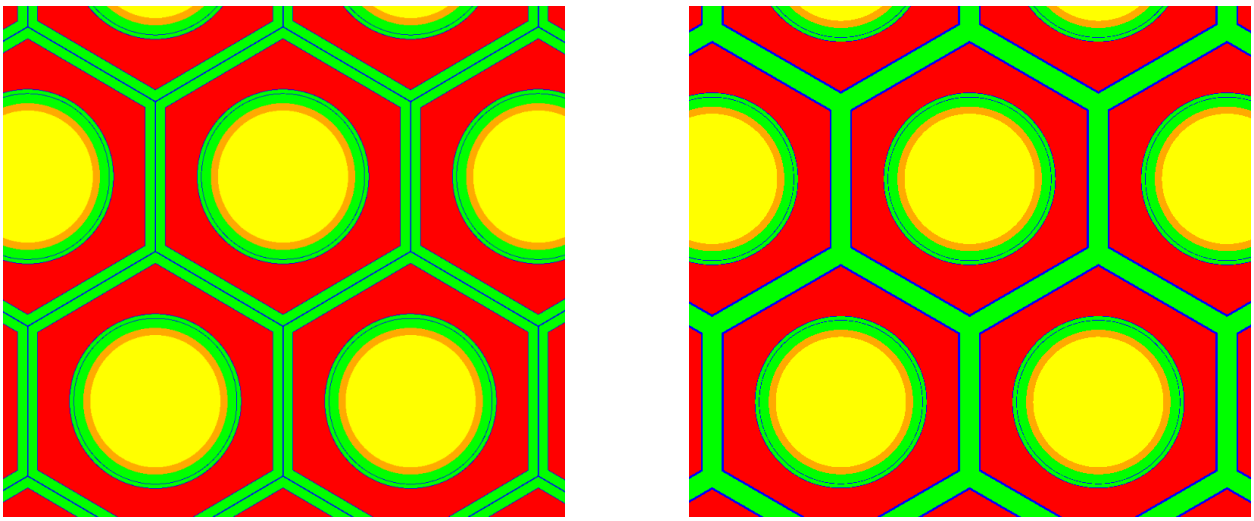

(a) Before expansion **(b) After expansion**

Figure 8. SCALE visualization of radial view of the fueled region of the core showing the gap closure between the fuel elements.

Feedback Verification Results

The results of each of these thermal expansion studies are shown in Table 10. For the Doppler, fuel elongation, and reflector thermal expansion coefficients, the SCALE model is in good agreement with the reference MCNP model. Though the standalone SS316 clad thermal expansion comparison was not performed, the total overall feedback effect demonstrates good agreement. The radial alumina thermal expansion was capable of being performed independently of all other radial expansions, so this value is included in Table 10 for comparison—but it was not included in determining the total temperature feedback. Differences in these feedback results are likely caused by the exact thermal expansion temperatures and coefficients in the reference models being unknown. For example, the Doppler coefficient calculated from Figure 6 varies according to the point of reference from −0.1022 to −0.0736 cents/K at the lower to the upper operating temperature range, respectively. However, the Doppler coefficient determined at 1,061.17 K was used for comparison in Table 10.

3.2 VALIDATION

While the code-to-code verification results presented above provide confidence in the model, the validation studies presented here are compared with actual experimental results. The eigenvalue bias was estimated via measured bias of experiments that were found to be similar to INL Design A. The decay heat calculations were validated by comparison to ^{235}U burst fission experiments.

Table 10. Full-core temperature coefficients of reactivity feedback

Feedback Effect (cents/K)	Ref. MCNP	SCALE
Doppler	−0.1074	−0.0744 ± 0.0013
UO_2 Fuel Axial Elongation	−0.0422	−0.0343 ± 0.0023
Alumina Reflector Radial Thermal Expansion	−0.0225	−0.0263 ± 0.0028*
Outer SS316 Fuel Clad Thermal Expansion	−0.0323	-
All Radial Expansions (Clad, Reflector, and CDs)	-	−0.0621 ± 0.0028
TOTAL	−0.2044	−0.1708 ± 0.0039

* Value not included in total. Provided for comparison purposes only.

3.2.1 EIGENVALUE VALIDATION

The SCALE module TSUNAMI-IP was used to compare the INL Design A model with criticality experiments of the International Criticality Safety Benchmark Evaluation Project (ICSBEP) Handbook [25]. The SCALE input files were taken from the VALID library, which contains more than 600 reviewed SCALE input files for ICSBEP experiments and is used for the SCALE library validation for criticality safety analysis [26], [27]. These experiments cover a wide range of characteristics, including different physical fuel forms, fissile materials, and spectral conditions. Using energy-dependent sensitivity coefficients generated using CE KENO, TSUNAMI-IP generates an integral index, c_k, that estimates the similarity between two critical systems in terms of related uncertainty from nuclear data and is used for criticality code validation. c_k is normalized such that a value of 1.0 represents complete similarity between the SCALE model and the critical experiment, whereas a value of 0.0 represents no similarity. Values of $c_k > 0.9$ indicate significant similarity to determine applicable validation experiments. For the INL Design A SCALE model at BOL cold zero power, 25 critical experiments had similarity indices greater than 0.9. Although extending the available experiments to all ICSBEP cases leads to 143 with similarity indices greater than 0.9, only the 25 contained within VALID were considered. These 25 experiments are listed in Appendix B. For these 25 critical experiments, the corresponding SCALE models showed a bias of 200 pcm +/- 400 pcm in eigenvalue which is a reasonable result. Because of the large similarity of the SCALE INL Design A model to these experiments, it can be concluded that the bias for the INL Design A calculations with SCALE is in a similar range.

3.2.2 DECAY HEAT VALIDATION

ORIGEN is the SCALE module responsible for both depletion and decay. Therefore, it is desirable to validate ORIGEN for decay heat calculations. For the INL Design A core, roughly 90% of all fissions occur in ^{235}U. The remaining 10% occur in ^{238}U, with a negligible amount coming from Pu isotopes. At shutdown, decay heat produces 0.339 MW, or 6.78% of the total thermal power. Following shutdown, roughly 92% of the cumulative energy release occurs within the first 24 hours. Therefore, the ability to accurately model the decay heat of ^{235}U fission products in the first day following shutdown is very important in this system. To validate the decay heat predicted in SCALE, comparisons were made to a series of burst fission, or pulse fission, experiments. These experiments measure the energy release over time following a single fission of ^{235}U. These measurements typically occur over a time period less than a day following the fission. A plot comparing multiple burst fission energy release experiments and the SCALE simulation is shown in Figure 9. The smooth blue curve titled `origen` is the SCALE prediction of the decay heat curve, whereas the other datasets are the experimental measurements shown with 2-σ error bars and are described in [28]. The most accurate experiments have 1-σ uncertainties in the 2–3% range. As seen in Figure 9, the `origen` prediction agrees well with the measurements and is within two standard deviations for almost all data

points. Based on this analysis, the SCALE prediction of instantaneous decay heat for the INL Design A model has a 1% +/- 2% bias. This good agreement serves as a partial validation of SCALE and its analysis of the INL Design A core; a full validation would require a comparison between the SCALE total decay heat and actual measured INL Design A decay heat.

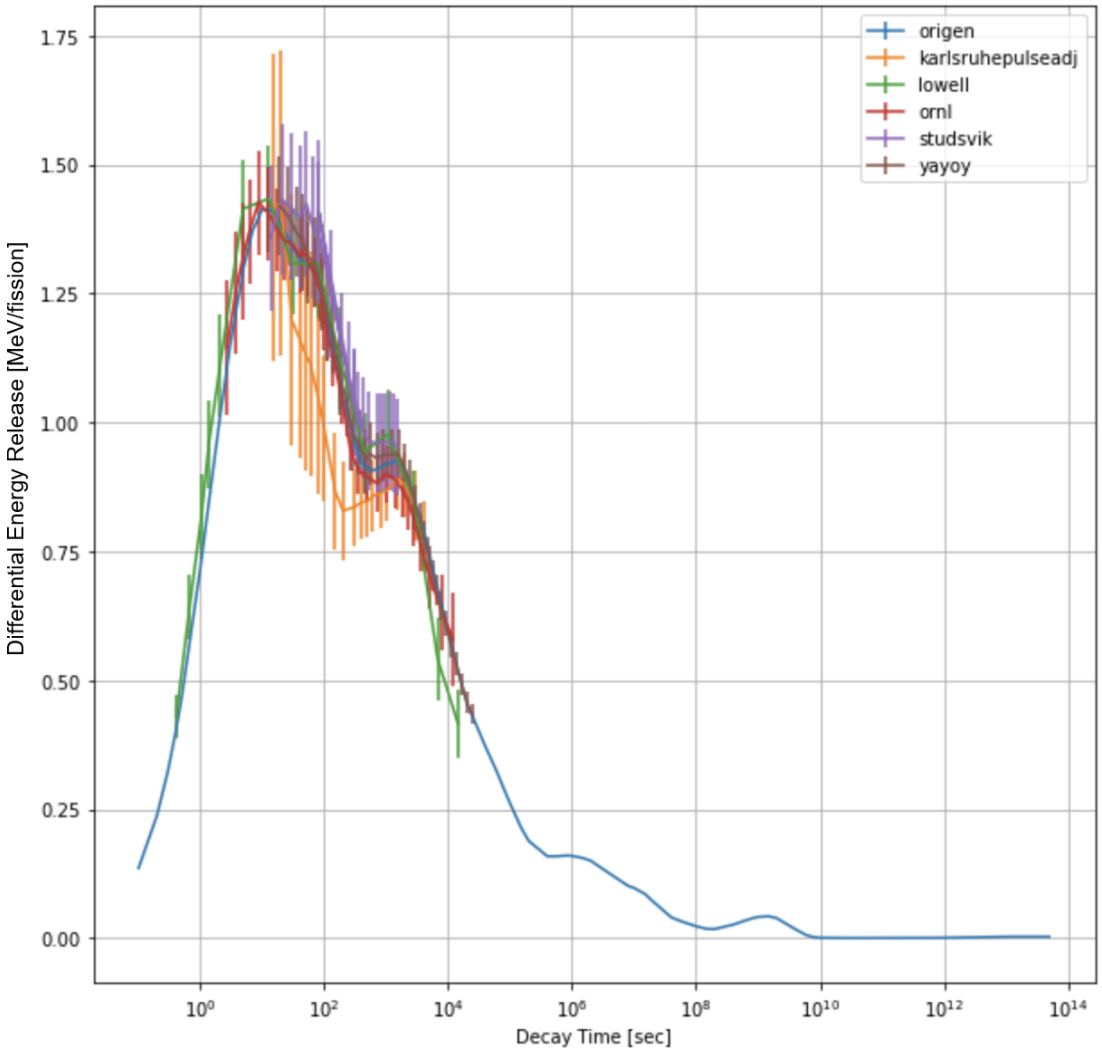

Figure 9. Decay heat verification comparison between SCALE and burst fission experiment measurements for ^{235}U.

4. RESULTS

Confidence was established in the SCALE INL Design A model, the approach, and the calculated results using the results outlined in the previous section. The model was then used to generate data that can be used as input to MELCOR. The following sections outline the results of some of these simulations. All results presented here used the SCALE Standard Composition Library and CE ENDF/B-VII.1 data.

4.1 POWER PROFILES

As described in Section 2.2, the model initially had a flat temperature distribution. The resulting power distribution was then used to create a temperature distribution in MELCOR (given in Table 6) which was used to inform a second iteration in SCALE. The resulting normalized power distributions from this second iteration are shown in Figure 10 at both BOL and after the five-year core lifetime. Though the material definition, cross section library, and temperature distribution differ from the reference document, the axial power distributions from the INL reference and the original Megapower design are shown alongside the SCALE profiles. The power profile from the INL reference represents the hottest fuel element in the core, whereas the SCALE and LANL curves are core averages. All curves demonstrate fundamental agreement with each other despite these differences. Because of the axial BeO reflectors located directly above and below the active fuel region of the core, there are significant reflector peaks at the top and bottom of the core. The SCALE model captures these peaks better than the other profiles, likely due to a finer axial mesh compared to the MCNP models. Though the BeO reflector thicknesses are the same in both the top and bottom of the core, the perforations in the upper reflector by the heat pipes lead to a reduction in overall reflector material. This causes the upper reflector peak to be less pronounced than the lower peak, where the reflector is intact. Though it is difficult to see in Figure 10, both SCALE profiles are located almost directly on top of each other. This is because, even after five years at full power, discharge burnup is not significant enough to cause a shift in the power distribution.

Additionally, a similar plot was made in the radial direction showing the power profile at both BOL and after five years. This is shown in Figure 11. Like in the axial plot, both curves are nearly on top of each other due to the low discharge burnup of the system after five years.

4.2 CROSS SECTION LIBRARY COMPARISON

As part of the ongoing work in SCALE to support advanced reactor modeling, a new 302-group fast-spectrum library was developed [29]. This MG library was optimized for sodium-cooled fast reactors but was tested using the INL Design A model to determine its applicability for HPRs. The eigenvalue differences between this new 302-group MG library and the ENDF/B-VII.1 CE library over the five-year core lifetime are shown in Table 11. All cases were converged to less than 10 pcm eigenvalue uncertainty. Over the core lifetime, use of the 302-group library adds only a small bias of 176.36 pcm on average.

Table 11. Full-cycle comparison between 302-group fast-spectrum library and ENDF/B-VII.1 CE library

Years	0.00	0.01	0.42	0.84	1.25	1.67	2.08	2.50	2.92	3.33	3.75	4.17	4.58	5.00
Δk (MG-CE) (pcm)	174	171	188	187	173	190	166	191	168	164	160	170	186	181

Furthermore, it was of interest to investigate the impact of the ENDF/B nuclear data library evaluation. A study was performed that determined the differences in eigenvalue between using the ENDF/B-VII.1

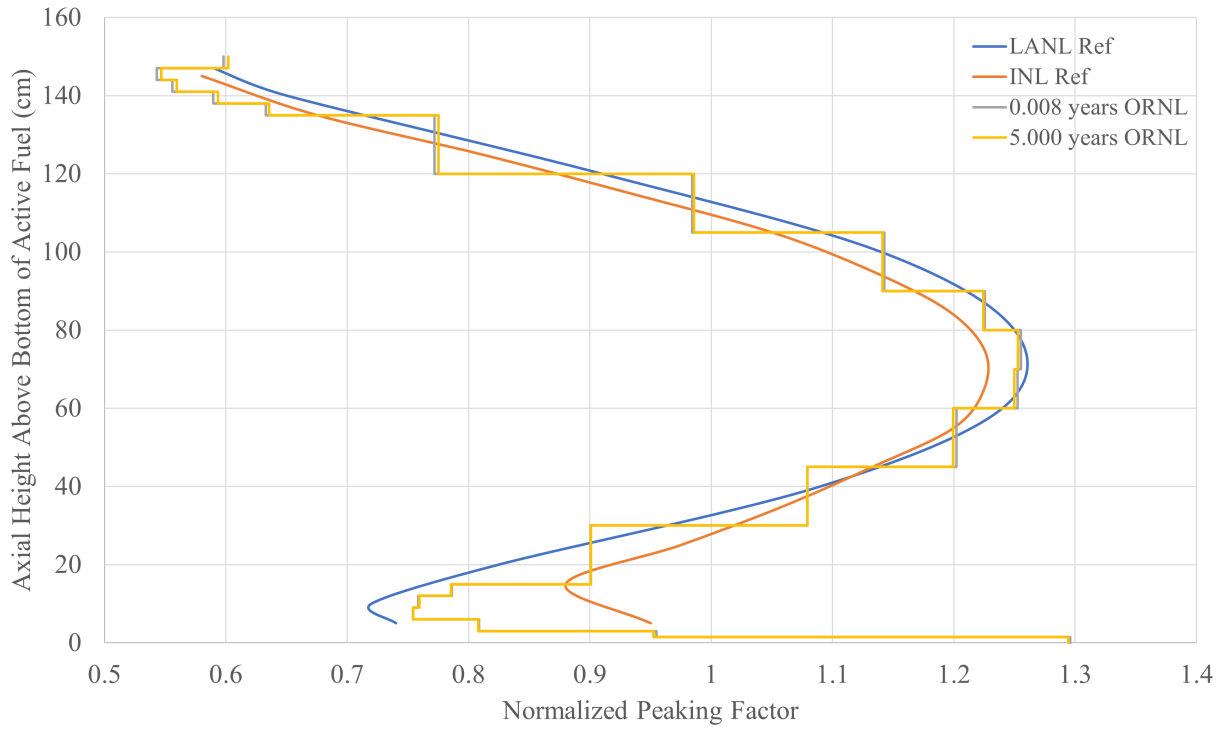

Figure 10. Axial power profiles at both BOL and after five years. INL and Megapower profiles are also shown for comparison.

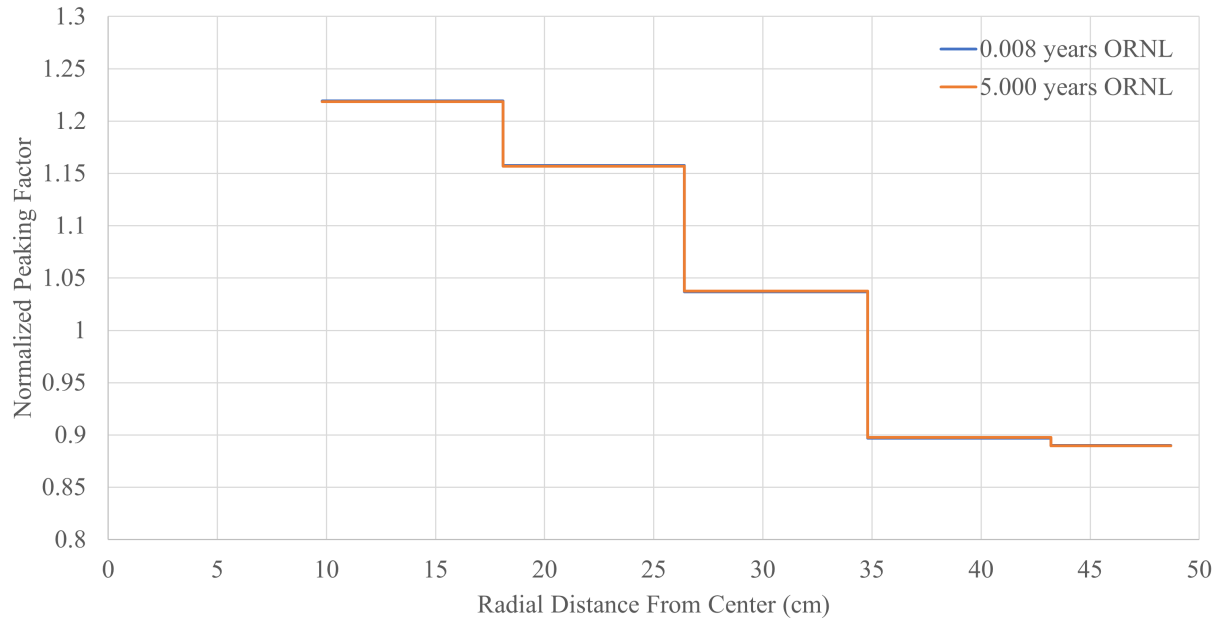

Figure 11. Radial power profiles at both BOL and after five years.

and new ENDF/B-VIII.0 CE libraries over the core lifetime. The results of this comparison are given in Table 12. On average, substituting the ENDF/B-VIII.0 library for the ENDF/B-VII.1 library leads to a 300 pcm reduction in eigenvalue. The observed eigenvalue differences are the combined effect of updates in the cross sections of various important cross sections in the ENDF/B-VIII.0 release compared to ENDF/B-VII.1. As an example, the neutron multiplicity of ^{235}U was updated, which directly contributes to the calculated multiplication factor. Other relevant reactions such as fission and neutron capture of ^{235}U and ^{238}U most likely also significantly contribute to the observed differences.

Table 12. Full cycle comparison between ENDF/B-VIII.0 and ENDF/B-VII.1 CE libraries

Years	0.00	0.01	0.42	0.84	1.25	1.67	2.08	2.50	2.92	3.33	3.75	4.17	4.58	5.00
Δk (VIII.0-VII.1) (pcm)	−311	−307	−286	−307	−292	−303	−325	−300	−303	−328	−305	−301	−293	−292

4.3 DECAY HEAT AND ACTIVITY EXAMPLES

The masses, activities, and decay heat values for all tracked isotopes within SCALE were generated using the developed INL Design A full-core model. These data were then post-processed and formatted into MELCOR input files to be used as source terms for severe accident analysis. Some examples of the types of data of interest are presented here.

A plot showing the top ten decay heat producing isotopes during the first ten days following shutdown at 2 GWd/MTIHM is shown in Figure 12. The largest contributors to the overall decay heat over this time frame are ^{140}La, ^{144}Pr, and ^{239}Np. Total decay heat for these ten isotopes is shown as the "Subtotals" curve, whereas the total decay heat for all tracked SCALE isotopes is shown as the "Totals" curve.

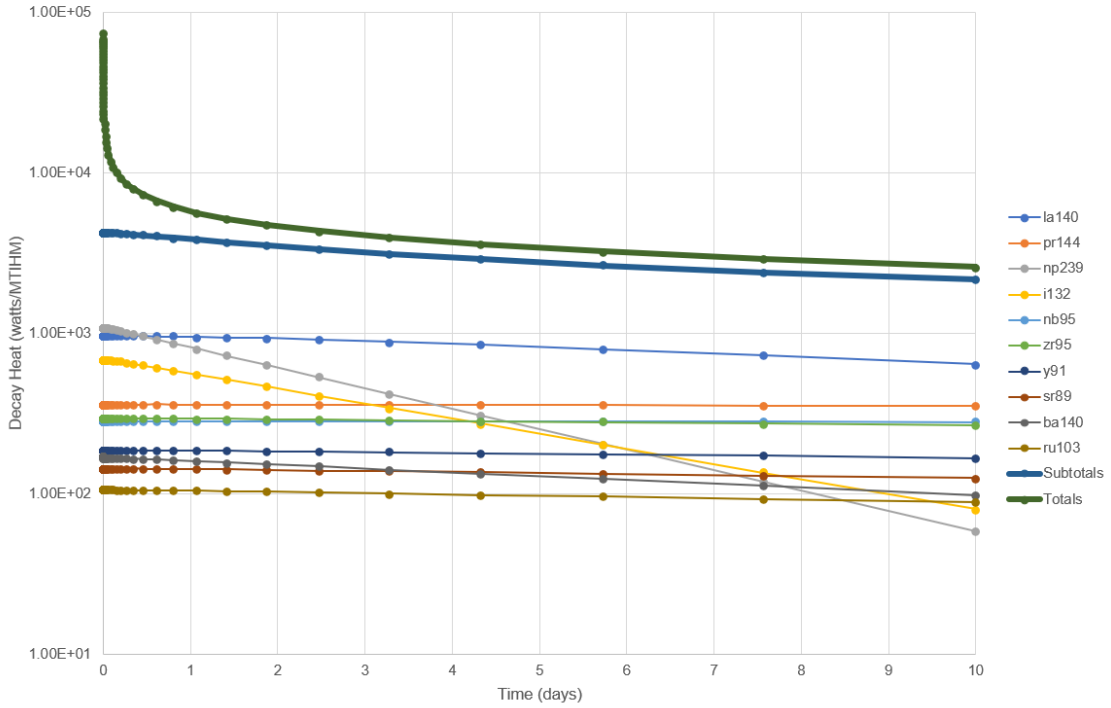

Figure 12. Decay heat for select isotopes at 2 GWd/MTIHM.

Similarly, plots of specific activity can be plotted for any isotope that SCALE tracks. The activity during the first ten days following shutdown at 2 GWd/MTIHM for select iodine and cesium fission products is

shown in Figure 13. After the first ten days following shutdown, the activity of these isotopes is noticeably reduced, except that of ^{137}Cs.

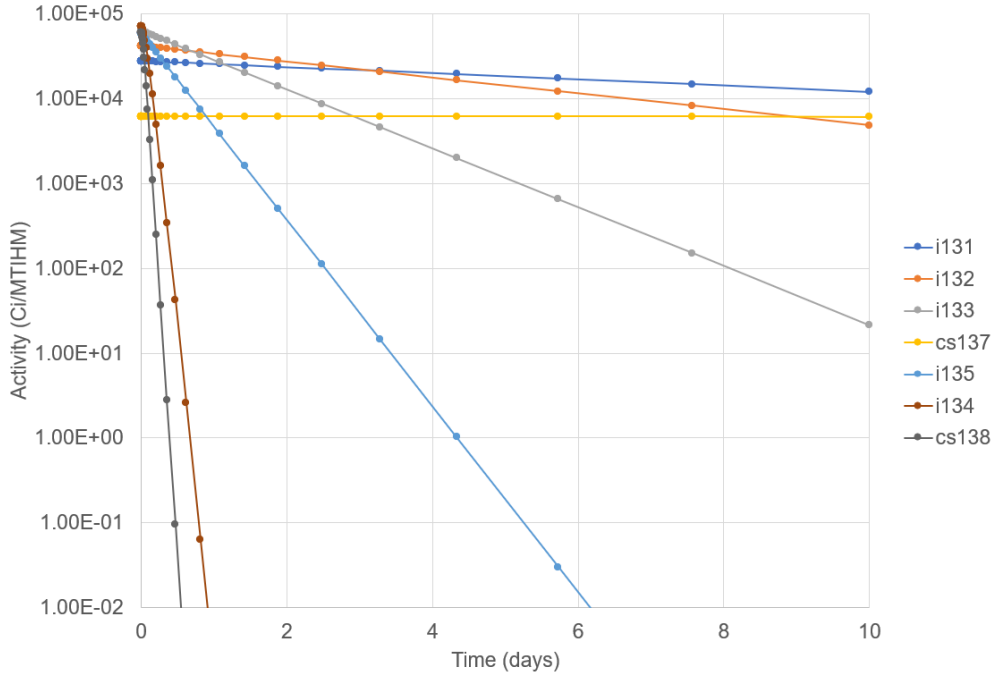

Figure 13. Activity for select Cs and I isotopes at 2 GWd/MTIHM.

4.4 SCALING DECAY HEAT

When looking at the HPR decay heat curves in Figure 12, the total decay heat is significantly lower than what would be expected of a typical pressurized water reactor (PWR). This is due to the lower specific power of the INL Design A reactor, which is roughly 2.7% that of a standard PWR core. Figure 14 shows a decay heat comparison between the SCALE INL Design A model and a typical PWR at two different discharge burnups. The PWR at a burnup of 2 GWd/MTIHM was chosen to match the INL Design A burnup. The PWR at a burnup of 60 GWd/MTIHM was added because it is a typical PWR discharge burnup. Even with identical burnups, the INL Design A decay heat is substantially lower than that of the PWR due to the lower core-specific power.

Though the shapes of the INL Design A and PWR decay heat curves appear similar, when scaled by specific power, they exhibit significant differences, as seen in Figure 15. At time $t = 0$, the INL Design A decay heat is 13.2% higher than the scaled PWR decay heat and becomes -10.0% at 1.88 days after shutdown. These large differences and fluctuations are likely due to the different in spectrum between an LWR and the HPR and demonstrate that the INL Design A decay heat curve cannot be approximated by scaling a standard PWR curve without incurring significant errors.

4.5 CONTROL DRUM ROTATION

Though there is sufficient worth in the 12 control drums to shut down the reactor (as shown in Table 8), their intended function is to compensate for excess reactivity control throughout reactor life. The effect of the control drum rotation angle on the core eigenvalue is shown in Figure 16 with both shutdown control rods inserted and removed. As expected, the curves are asymptotic at 0° and 180° due to the symmetric nature of the core. The reference document [21] states that the critical control drum rotation is 65°, which is very close to where the "Rods Out" curve intersects the 1.00 k_{eff} gridline.

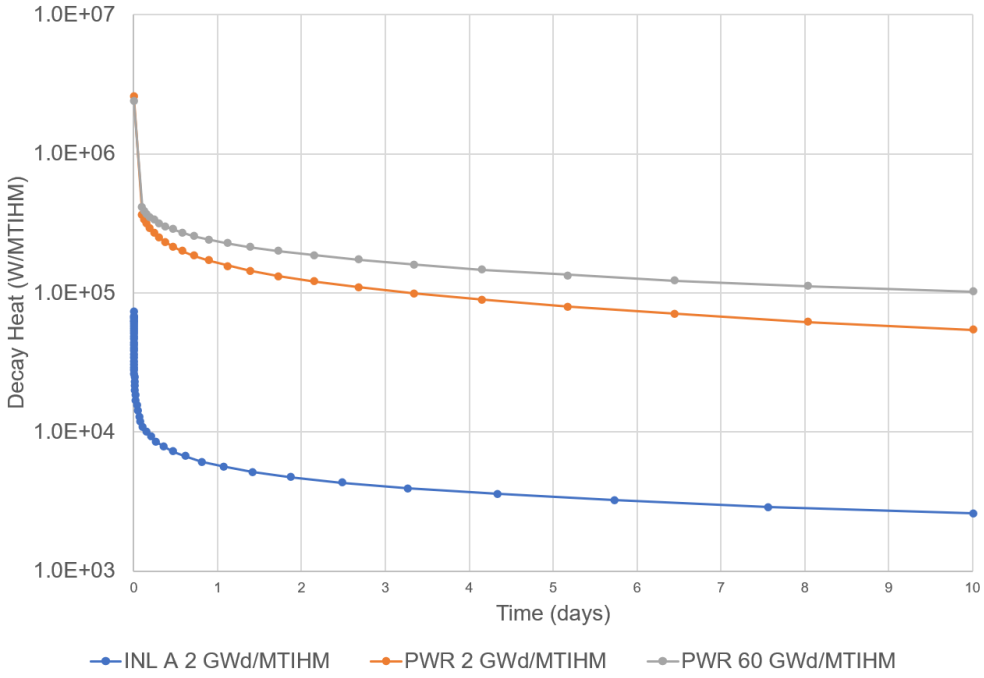

Figure 14. Specific decay heat comparison of INL Design A and two PWR burnups over the first 10 days following shutdown.

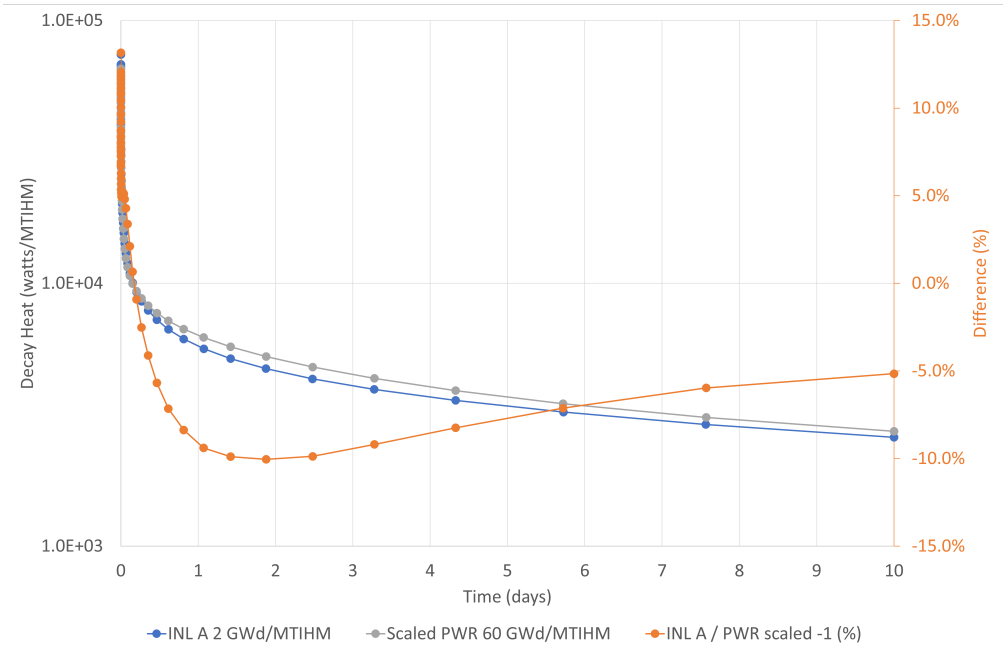

Figure 15. Specific decay heat differences between INL Design A and scaled PWR 60 GWd/MTIHM decay heat curve.

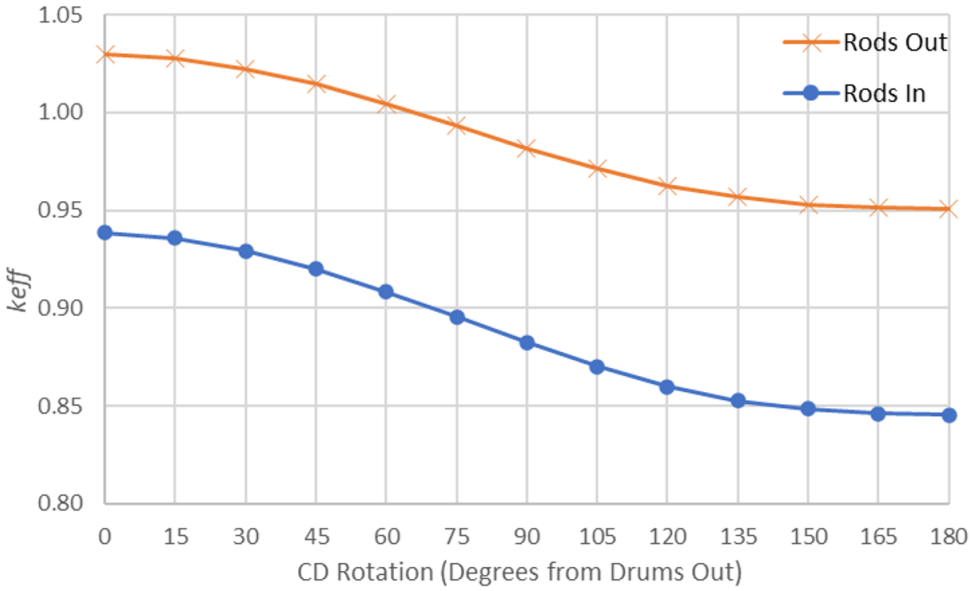

Figure 16. Eigenvalue as a function of control drum rotation angle with both shutdown rods inserted and removed.

5. CONCLUSIONS

This paper documents the results of modeling a fast-spectrum HPR using SCALE. Because of the increased interest in HPRs, reactor behavior during severe accident scenarios must be accurately modeled and predicted. This work was performed as part of the US NRC–led project to assess the modeling and simulation capabilities for accident progression, source term, and consequence analysis for non-LWR technologies. In a collaboration between the NRC, SNL, and ORNL, SCALE was used to provide pertinent core data to the MELCOR severe accident analysis code developed and managed by SNL. The models developed in this work were used to generate isotopic inventories, power distributions, decay heat data, and kinetics parameters to be used at the initiation of severe accident modeling in MELCOR.

The models used in this work were developed based on the INL Design A HPR microreactor. While these models incorporated most of the details outlined in the reference document [21], there were a few key material and modeling differences between the two due to incomplete information in the reference document. The SCALE models were built using both the isotopic number densities for each material that are listed in the reference document as well as using the predefined material compositions as available through the SCALE Standard Composition Library. Another key difference is the choice of CE nuclear data library; the reference results were generated with ENDF/B-VII.0 data while the results presented here were generated using the newer ENDF/B-VII.1 library because ENDF/B-VII.1 is SCALE's current standard nuclear data library. The SCALE models were generated with 100 spatially discretized fuel regions, 20 axial and 5 radial, to generate power profiles and spatially dependent isotopics. These models also used a fuel temperature distribution, which was provided by MELCOR, instead of a flat temperature profile.

These models were verified via comparisons with results presented in the reference document. Infinite lattice unit cell calculations were within approximately 50 pcm from the reference values when using identical isotopics and cross section libraries. Using the SCALE material definitions and the updated ENDF/B-VII.1 library, these calculations were within 99 pcm. The full core model was also verified, with eigenvalue differences of less that 200 pcm and reactivity worth differences of 3.5% or less. Doppler broadening and both axial and radial thermal expansion coefficients were calculated and compared to reference values. Though a direct comparison for the radial thermal expansion coefficient was not possible, these temperature coefficients of reactivity feedback agreed well with the reference values and the overall feedback effect.

The SCALE model results were validated using two different experimental techniques. The bias in the decay heat calculation was determined to be 1% +/- 2% using burst fission experiments. The eigenvalue bias at BOL cold zero power was determined using 25 critical experiments for which a similarity to the INL Design A was found using a similarity coefficient of greater than 0.9. The bias of 200 pcm +/- 400 pcm found for these experiments indicates a similar bias for the results obtained for INL Design A.

The SCALE spatial discretization allowed for a detailed axial power profile. The lower reflector peak was more pronounced than what was seen in the reference due to a finer discretization in the lower fuel region. For the same reason, the presence of an upper reflector peak was captured which was otherwise missed by the reference model. These power profiles were generated as a function of time as the core depleted. It was found that, due to the low discharge burnup of this design, there is no significant change in the axial or radial power profiles throughout the core lifetime.

With the SCALE models both verified and validated, they were successfully used to generate the isotopic inventories, power distributions, decay heat data, and kinetics parameters for the MELCOR severe accident analysis code. The results of the MELCOR analysis are provided in a different report [1].

REFERENCES

[1] K. Wagner, C. Faucett, R. Schmidt, and D. Luxat, "MELCOR Accident Progression and Source Term Demonstration Calculations for a Heat Pipe Reactor," Sandia National Laboratories, Albuquerque, NM, Tech. Rep. SAND2021-6732 PE, Jun. 2021.

[2] U.S. Department of Energy: Office of Nuclear Energy. (2021). What is a Nuclear Microreactor? [Online]. Available: https://www.energy.gov/ne/articles/what-nuclear-microreactor.

[3] M. Anastasio, P. Kern, *et al.*, "Task Force of Energy Systems for Forward/Remote Operating Bases," Department of Defense: Defense Science Board, Washington, D.C., Tech. Rep., Aug. 2016.

[4] B. H. Yan, C. Wang, and L. G. Li, "The technology of micro heat pipe cooled reactor: A review," *Annals of Nuclear Energy*, vol. 135, Jan. 2020. DOI: 10.1016/j.anucene.2019.106948.

[5] G. Hu, R. Hu, J. M. Kelly, and J. Ortensi, "Multi-Physics Simulations of Heat Pipe Micro Reactor," Argonne National Laboratory, Lemont, IL, Tech. Rep. ANL-NSE-19/25, Sep. 2019.

[6] Y. Ma, M. Liu, E. Chen, B. Xie, X. Chai, S. Huang, K. Wang, and H. Yu, "RMC/ANSYS Multi-physics Coupling solutions for Heat Pipe Cooled Reactors Analyses," in *PHYSOR 2020*, Cambridge, United Kingdom, Mar. 2020.

[7] P. Sabharwall, C.-S. Lin, J. Hansel, V. Laboure, D. Andrs, W. Hoffman, S. Novascone, A. Slaughter, and R. Martineau, "Application of Integrated Modeling and Simulation Capabilities for Full Scale Multiphysics Simulation of Microreactor Concepts," Idaho National Laboratory, Idaho Falls, IL, Tech. Rep. INL/EXT-19-55159, Aug. 2019.

[8] H. Guo, K. Y. Feng, H. Y. Gu, X. Yao, and L. Bo, "Neutronic modeling of megawatt-class heat pipe reactors," *Annals of Nuclear Energy*, vol. 154, May 2021. DOI: 10.1016/j.anucene.2021.108140.

[9] Westinghouse. (2021). eVinci™ Micro Reactor, [Online]. Available: https://www.westinghousenuclear.com/new-plants/evinci-micro-reactor.

[10] Y. Arafat and J. van Wyk, "eVinci™ Micro Reactor," *Nuclear Plant Journal*, pp. 34–37, Mar.–Apr. 2019.

[11] A. Maioli, H. L. Detar, R. L. Haessler, B. N. Friedman, C. A. Belovesick, J. H. Scobel, S. T. Kinnas, M. C. Smith, J. van Wyk, and K. Fleming, "Westinghouse eVinci™ Micro-Reactor Licensing Modernization Project Demonstration," Southern Company, Tech. Rep. EMR_LTR_190010, Aug. 2019.

[12] Oklo LLC. (2021). Oklo, [Online]. Available: https://oklo.com/.

[13] U.S. NRC. (2020). Aurora – Oklo Application, [Online]. Available: https://www.nrc.gov/reactors/new-reactors/col/aurora-oklo.html.

[14] U.S. NRC. (2020). NRC Non-Light Water Reactor (Non-LWR) Vision and Strategy, Volume 3 – Computer Code Development Plans for Severe Accident Progression, Source Term, and Consequence Analysis, [Online]. Available: https://www.nrc.gov/docs/ML2003/ML20030A178.pdf.

[15] W. A. Wieselquist, R. A. Lefebvre, and M. A. Jessee, "SCALE Code System," Oak Ridge National Laboratory, Oak Ridge, TN, Tech. Rep. ORNL/TM-2005/39, Apr. 2020.

[16] L. Humphries, B. Beeny, F. Gelbard, D. Louie, and J. Phillips, "MELCOR Computer Code Manuals - Vol. 1: Primer and Users' Guide," Sandia National Laboratories, Albuquerque, NM, Tech. Rep. SAND2017-0455 O, Jan. 2017.

[17] NASA. (2021). Kilopower, [Online]. Available: https://www.nasa.gov/directorates/spacetech/kilopower.

[18] M. A. Gibson, S. R. Oleson, D. I. Poston, and P. McClure, "NASA's Kilopower Reactor Development and the Path to Higher Power Missions," in *2017 IEEE Aerospace Conference*, Big Sky, MT, Mar. 2017.

[19] P. R. McClure, D. I. Poston, V. R. Dasari, and R. S. Reid, "Design of Megawatt Power Level Heat Pipe Reactors," Los Alamos National Laboratory, Los Alamos, NM, Tech. Rep. LA-UR-15-28840, Nov. 2015.

[20] J. W. Sterbentz, J. E. Werner, M. G. McKellar, A. J. Hummel, J. C. Kennedy, R. N. Wright, and J. M. Biesdorf, "Special Purpose Nuclear Reactor (5 MW) for Reliable Power at Remote Sites Assessment Report," Idaho National Laboratory, Idaho Falls, ID, Tech. Rep. INL/EXT-16-40741, Apr. 2017.

[21] J. W. Sterbentz, J. E. Werner, A. J. Hummel, J. C. Kennedy, R. C. O'Brien, A. M. Dion, R. N. Wright, and K. P. Ananth, "Preliminary Assessment of Two Alternative Core Design Concepts for the Special Purpose Reactor," Idaho National Laboratory, Idaho Falls, ID, Tech. Rep. INL/EXT-17-43212, May 2018.

[22] T. Goorley *et al.*, "Initial MCNP6 Release Overview," *Nuclear Technology*, vol. 180, pp. 298–315, Dec. 2012.

[23] A. E. Waltar, D. R. Todd, and P. V. Tsvetkov, *Fast Spectrum Reactors*. New York, USA: Springer Science & Business Media, 2012, ISBN: 978-1-4419-9571-1.

[24] Syalons. (2021). Alumina, [Online]. Available: https://www.syalons.com/materials/alumina/.

[25] NEA, "International Handbook of Evaluated Criticality Safety Benchmark Experiments," Organisation for Economic Co-operation and Development/Nuclear Energy Agency, Tech. Rep. NEA-1486/18, 2020.

[26] E. M. Saylor, W. J. Marshall, J. B. Clarity, Z. J. Clifton, and B. T. Rearden, "Criticality Safety Validation of SCALE 6.2.2," Oak Ridge National Laboratory, Oak Ridge, TN, Oak Ridge, TN, Tech. Rep. ORNL/TM-2018/884, 2018. [Online]. Available: https://www.osti.gov/servlets/purl/1479759.

[27] W. J. Marshall and B. T. Rearden, "The SCALE Verified, Archived Library of Inputs and Data – VALID," in *ANS NCSD 2013, Wilmington, NC, September 29 – October 3*, 2013, pp. 319–329, ISBN: 9781629938165.

[28] G. Ilas, J. Burns, B. Hiscox, and U. Mertyurek, "SCALE 6.2.4 Validation: Reactor Physics," Oak Ridge National Laboratory, Tech. Rep. ORNL/TM-2020/1500/v3, 2021.

[29] F. Bostelmann, B. T. Rearden, W. Zwermann, and A. Pautz, "SCALE/AMPX Multigroup Libraries for Sodium-Cooled Fast Reactor Systems," *Annals of Nuclear Energy*, vol. 140, Jun. 2020. DOI: 10.1016/j.anucene.2019.107102.

APPENDIX A. INPUTS AND ADDITIONAL INFORMATION

APPENDIX A. INPUTS AND ADDITIONAL INFORMATION

All inputs and data used in this work were generated using publicly available information and contained no proprietary data whatsoever. Therefore, the SCALE input and output files have been made publicly available at https://code.ornl.gov/scale/analysis/non-lwr-models-vol3. The results of these SCALE analyses were provided to the MELCOR team. A description of the MELCOR models and results can be found in Wagner et al. [1].

APPENDIX B. VALIDATION EXPERIMENTS

APPENDIX B. VALIDATION EXPERIMENTS

The 25 critical experiments used in Section 3.2.1 are shown in Table 13. All experiments were taken from VALID and had metallic fuel and fast neutron spectrums.

Table 13. The 25 VALID critical experiments with similarity indices greater than 0.9

Experiment Name
HEU-MET-FAST-005-002
HEU-MET-FAST-005-003
HEU-MET-FAST-005-004
HEU-MET-FAST-005-005
HEU-MET-FAST-005-006
HEU-MET-FAST-016-001
HEU-MET-FAST-016-002
HEU-MET-FAST-017-001
HEU-MET-FAST-030-001
HEU-MET-FAST-038-001
HEU-MET-FAST-038-002
HEU-MET-FAST-052-001
HEU-MET-FAST-094-001
HEU-MET-FAST-094-002
IEU-MET-FAST-003-001
IEU-MET-FAST-003-001S
IEU-MET-FAST-004-001
IEU-MET-FAST-004-001S
IEU-MET-FAST-005-001
IEU-MET-FAST-005-001S
IEU-MET-FAST-006-001
IEU-MET-FAST-008-001
IEU-MET-FAST-009-001
IEU-MET-FAST-019-001
IEU-MET-FAST-019-002